A Demodulation Scheme Based on Measuring Interference Fringe Visibility With a Highly Birefringent Fiber Based Michelson Interferometer

Liang Zhang, Zijue Zhu, Tianyu Yang, Wei Chen [2], and Yuming Dong

***Abstract*—We propose a novel demodulation scheme based on measuring interference fringe visibility and demonstrate it using a typical Michelson interferometer (MI) configuration. The key component to achieve the scheme is a section of highly birefringent fiber (HBF) spliced into the sensing arm to function as the sensing element. The optical path difference (OPD) leads to interference fringes, while the birefringence of the HBF results in a visibility envelop. It is possible to detect measurands associated with birefringence through measuring the visibility, which is attributed to a flexible use of the fundamental principle of interferometry. As one of the potential applications, temperature sensing employing the MI configuration is performed. Moreover, the technique has the advantage of being immune to element instabilities, such as power fluctuation of the light source, phase shift of the reference arm, noise of the photo detector, and wavelength shift of the optical spectrum analyzer (OSA). This work may provide an alternative method to achieve high precision interferometry with low cost.**

***Index Terms*—Demodulation, visibility, michelson interferometer, fiber sensing.**

I. Introduction

OPTICAL fiber, with the superiority of immunity to electromagnetic interference (EMI), high pressure resistance, low loss, low cost, lightweight, etc., has provided optic fiber sensor (OFS) with great research values [1]–[3]. Two beam interferometric OFS is a high precision measuring tool that enables us to extract the optical path difference (OPD) change at micro or even nanoscale from an interference pattern variation due to the coherent lasers and the tiny wavelength scale in the near infrared regime. It has diverse applications [4]–[7], such as infrasound detection [8], and inertial navigation [9], and state-of-the-art ocean bottom seismic cable (OBC) systems [10].

The fringe of two beam interferometer can be observed in spectral and time domain in the shape of a cosine function. Generally, three dominant features of the spectrum are used for quantitatively determining the measurands, including phase, intensity, and wavelength (frequency). As these three features are absolute values, demodulation accuracy is significantly affected by elements' instabilities, including but not necessarily limited to power fluctuation of the light source, phase shift of the reference arm, noise of the photon detectors, and wavelength shift of the optical spectrum analyzer (OSA). Aiming to improve demodulation accuracy, engineers utilized light sources and detectors with high stability [11], [12], or employed a standard reference element [13], which, nevertheless, greatly increases the cost and complexity of the system. Besides, numerous optimized demodulation algorithms such as Pound-Drever-Hall (PDH) technique [14], [15], wavelet threshold denoising [16], [17], and the spectral processing method [18]–[20], were employed to mitigate the problem to a certain extent but also increase complexity of systems. Consequently, how to achieve a low-cost, simple, and high precision demodulation scheme is still a quite challenge.

Surprisingly, we focus on a rarely considered feature of the fringe, the visibility, which is a relative value. Measurement of visibility benefits from immunities to the aforementioned elements' instabilities, and consequently overcomes the tradeoff between demodulation accuracy and system complexity. Furthermore, visibility can be easily measured by a wavelength swept laser, which is much cheaper than a high resolution OSA [21], [22].

Previously, we have presented a method of visibility modulation associated with strain sensing [23], [24]. In this paper, we propose a demodulation scheme based on measuring interference fringe visibility, and demonstrate it by a specially designed interferometric scheme, where a section of highly birefringent fiber (HBF) and highly reflecting fiber Bragg grating (FBG) are spliced together to function as the sensing element. In the interference spectrum, fringes are introduced by the OPD between the two arms, while the visibility is enveloped due to the birefringence of the HBF. Consequently, it can monitor the birefringence dependent measurands by measuring the visibility. The experimental results show that the visibility of the interference pattern is insensitive to power fluctuation of the light source, phase shift of the reference arm, and wavelength shift of the OSA. Temperature sensing employing this interferometer fiber system is presented as one of the potential applications.

Manuscript received May 8, 2021; revised June 13, 2021; accepted June 26, 2021. Date of publication June 30, 2021; date of current version July 19, 2021. This work was supported in part by the Shenzhen Research Foundation under Grant JCYJ20170413152328742 in part by National Key RD Program Funding project under Grant 2016YFB1200401, and in part by the National Natural Science Foundation of China under Grant 61 505 239. *(Corresponding author: Tianyu Yang.)*

Shenzhen Institute of Advanced Technology, Chinese Academy of Sciences, Shenzhen 518055, China, and also with the The Chinese University of Hong Kong, Hong Kong, China (e-mail: liang.zhang@siat.ac.cn; 317208215@qq.com; yangtianyu150@outlook.com; chenwei@siat.ac.cn; ym.dong@siat.ac.cn).

Digital Object Identifier 10.1109/JPHOT.2021.3093566

Calibration and comparison tests of the temperature sensor are also presented.

II. Principle of the Demodulation Scheme

Two beam fiber optic interferometer relies on coherent mixing of two optical signals, which are guided through the two arms. An interference fringe $I(f) = I_0(f) \times [1 + V(f)cos(\Delta\phi(f))]$ can be acquired as output, providing spectral and temporal information with features such as frequency f, phase $\Delta\phi(f)$, intensity $I(f)$. The visibility $V(f)$, which is directly affected by the polarization states of the two optical beams, generally shows no regular response to measurands. To the best of our knowledge, no demodulation scheme realized by measuring visibility has been reported. Here we develop a Michelson interferometer configuration to achieve a demodulation scheme based on measuring visibility.

When a section of HBF is inserted into the sensing arm as the sensing element, a phase delay between two orthogonal polarizations is generated due to the birefringence of the HBF. Thus, the interference fringe is divided into two parts:

$$I_x(f) = I_{0x}(f) \times [1 + V(f)cos(\Delta\phi(f))] \quad (1)$$

$$I_y(f) = I_{0y}(f) \times [1 + V(f)cos(\Delta\phi(f) + 2\pi BLf)] \quad (2)$$

where I_x and I_y represent the interference intensity on x and y polarization components respectively. B is the birefringence coefficient of the HBF. L is the length of the HBF.

The interference fringe obtained by the OSA is the sum of I_x and I_y, which can be expressed as the following equation:

$$\begin{aligned} I &= I_x(f) + I_y(f) \\ &= I_{0x}(f) \times [1 + V(f)cos(\Delta\phi(f))] + I_{0y}(f) \\ &\quad \times [1 + V(f)cos(\Delta\phi(f) + 2\pi BLf)] \\ &= I_{0x}(f) + I_{0y}(f) + [I_{0x}(f)V(f) + I_{0y}(f)V(f) \\ &\quad cos(2\pi BLf)]cos(\Delta\phi(f)) \\ &\quad - [I_{0y}(f)V(f)sin(2\pi BLf)]sin(\Delta\phi(f)) \\ &= I_{0x}(f) + I_{0y}(f) + V(f) \\ &\quad \sqrt{[I_{0x}(f)+I_{0y}(f)cos(2\pi BLf)]^2+[I_{0y}(f)sin(2\pi BLf)]^2} \\ &\quad \times cos[\Delta\phi(f) + \phi'(f)] \\ &= I'_0(f) \times [1 + V'(f)cos(\Delta\phi(f) + \phi'(f))] \end{aligned} \quad (3)$$

where we have (4), shown at the bottom of this page.

Since the interference fringe pattern obtained by the OSA is recorded in dBm unit, the visibility is expressed as follow:

$$10\lg I_{max} - 10\lg I_{min} = 10\lg\left(\frac{I_{max}}{I_{min}}\right) = 10\lg\left(\frac{1+V'(f)}{1-V'(f)}\right) \quad (5)$$

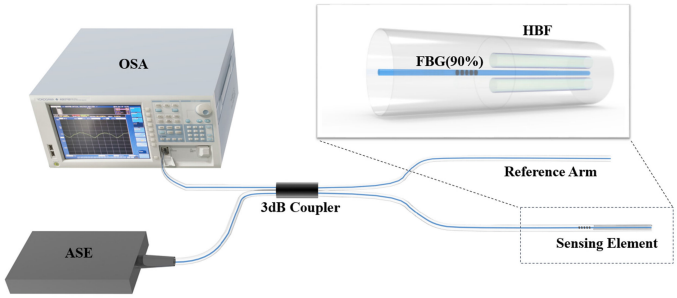

Fig. 1. The schematic diagram of the proposed fiber interferometric configuration.OSA: optical spectrum analyzer. ASE: amplified spontaneous emission. HBF: highly birefringent fiber. FBG: fiber Bragg grating.

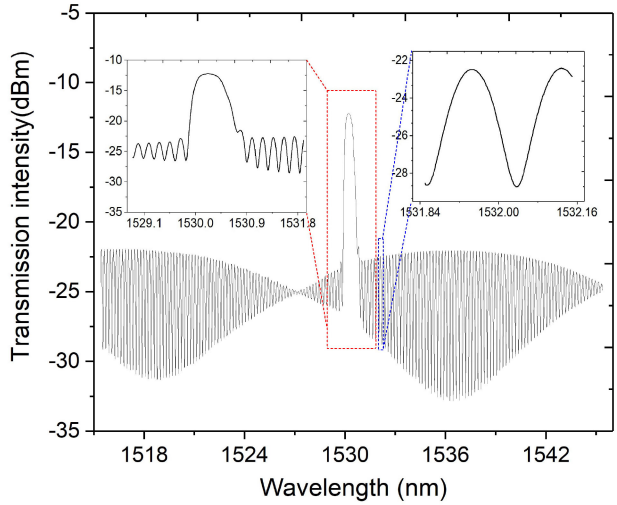

Fig. 2. A section of the interference pattern with a scanning span of 30 nm. The left and the right insets are the zoom-in spectrums of the red and the blue dotted frame area whose wavelength range are from 1528.9 nm to 1531.9 nm and from 1531.85 nm to 1532.15 nm, respectively. The data was achieved experimentally.

Thus, the visibility envelops interference fringes as a function of birefringence ($V'(f)$ vs B), which provides the opportunity to monitor birefringence dependent measurands (e.g., temperature and strain) by detecting visibility changes.

III. Results and Discussion

A. Feasibility Verification

To verify the feasibility of the proposed demodulation scheme, we conduct a temperature response test with a Michelson interferometer configuration as shown in Fig. 1. The ASE is an Erbium-doped fiber-based ASE. Its wavelength range and output power are 1527nm-1565 nm and about 20 dBm, respectively. A section of HBF (about 11.2 cm) with birefringence of 6×10^{-4} and a FBG with reflectivity of 90% are cascaded together as the sensing arm, while a single mode fiber acts as

$$V'(f) = V(f)\sqrt{[I_{0x}(f) + I_{0y}(f)cos(2\pi BLf)]^2 + [I_{0y}(f)sin(2\pi BLf)]^2}/[I_{0x}(f) + I_{0y}(f)] = F(B) \quad (4)$$

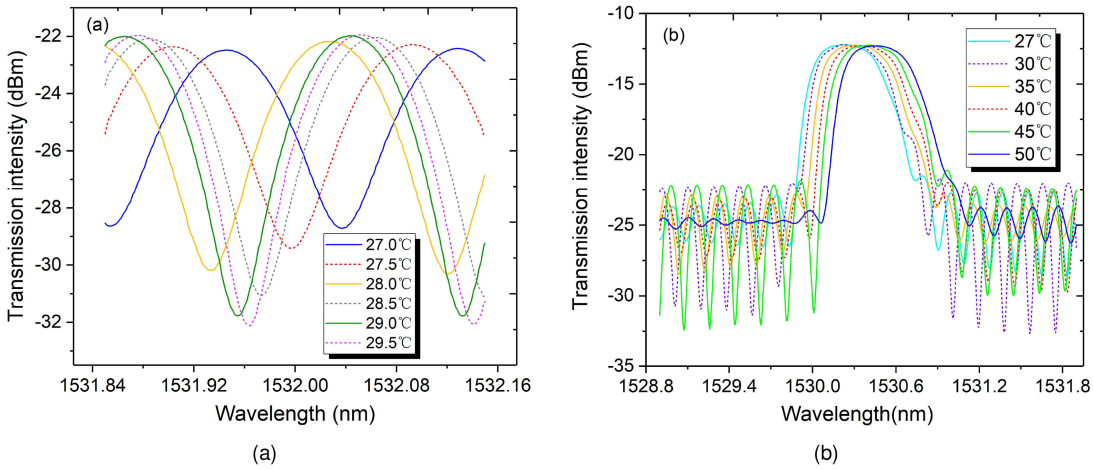

Fig. 3. (a) The transmission intensity within a narrow wavelength band for different temperatures ranging from 27.0 to 29.5 °C. (b) The transmission intensity around the Bragg wavelength as temperature increases from 27 to 50 °C.

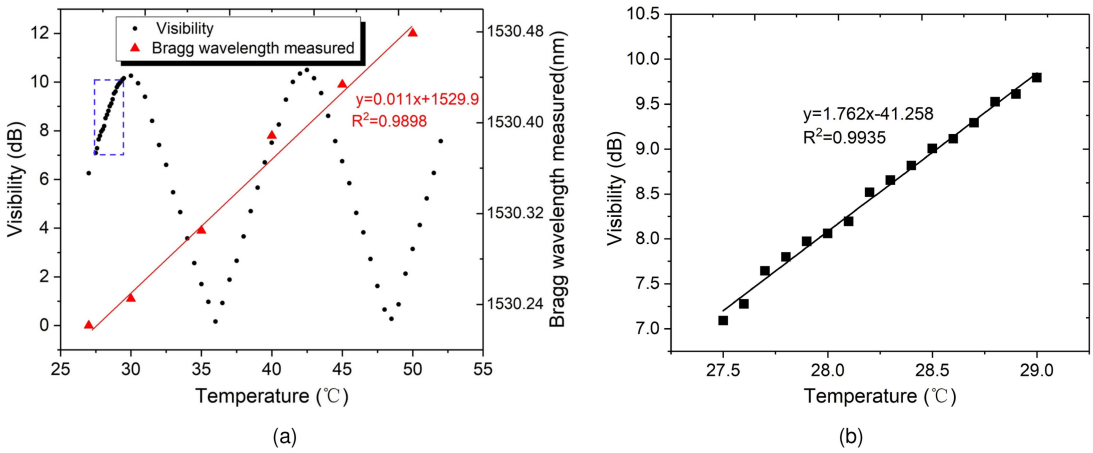

Fig. 4. (a) The responses of visibility within the temperature range from 27.5 to 29.0 °C. (b) The responses of visibility and Bragg wavelength within the temperature range from 27.0 to 52.0 °C.

the reference arm. The Bragg wavelength and 3 dB bandwidth of the FBG are about 1530.19 nm (25°C) and 0.57 nm, respectively. The fiber end faces of the two arms work as reflecting mirrors. The sensing arm is placed onto a temperature controller platform. The birefringence of the HBF and Bragg wavelength change with temperature. The output is observed by an OSA (Yokogawa, AQ6370D, resolution: 0.02 nm). All the data was achieved experimentally. Figure 2 presents the fringe visibility and the FBG reflection spectrum indicated in the blue and red dotted frame area, respectively. The Bragg wavelength can determine the rough temperature within a relatively wide range, but the sensitivity and resolution are limited. On the contrary, the visibility can be used to detect more precise temperature variation but suffers from period ambiguity. Combing these two parameters, both high resolution and large measurement range can be achieved.

The transmission intensity with the temperature increment of 0.5 °C is shown in Fig. 3(a). Meanwhile, as shown in Fig. 3(b), the shift of Bragg wavelength is simultaneously measured within the temperature range from 27 to 50 °C. The black dots and red triangles in Fig. 4(a) represent the responses of visibility and Bragg wavelength, which show an approximate cosine curve and a linear curve respectively. Figure. 4(b) shows the visibility response for different temperatures from 27.5 to 29.0 °C with an increment of 0.1 °C. The fitting curve indicates a sensitivity higher than 1.762 dB/°C. As the intensity resolution of the OSA is as high as 0.001 dB, the temperature measurement resolution can be higher than 5.675×10^{-4} °C, theoretically. It is noted that the visibility varies periodically respected to temperature. Longer HBF results in higher sensitivity but smaller period in the curve (visibility vs temperature), thus higher period ambiguity of visibility variation. To eliminate the period ambiguity of the visibility variation, the Bragg wavelength is employed to estimate the periodicity.

To illustrate the demodulation precision, the stability of the temperature platform is tested. Since the inherent fluctuation of temperature controller platform, the fluctuations at different temperatures are less than ±0.15°C. Further experimental validations of immunities to the power fluctuation of light source and the temperature shift of reference arm are performed. As shown in Figs. 5(a) and (b), the demodulated temperatures are quite stable for different powers and temperatures of reference

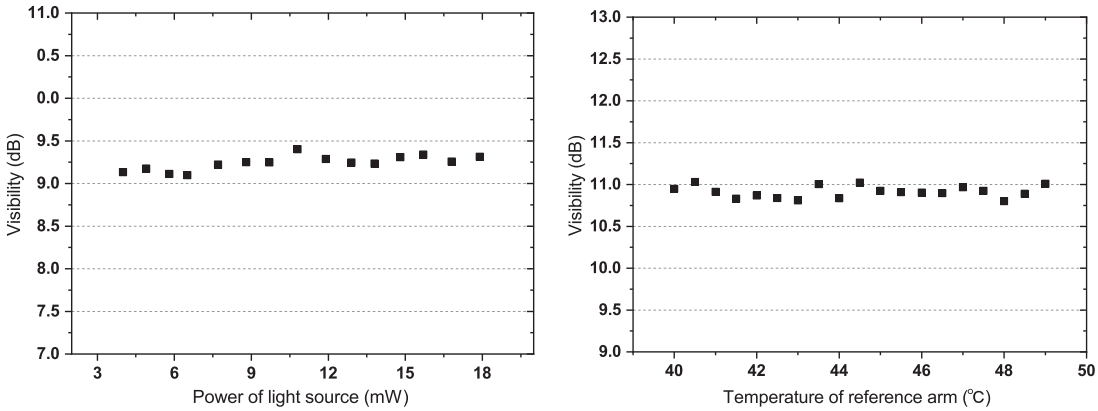

(a) (b)

Fig. 5. (a) The effect of power fluctuation on the demodulated temperature stability. (b) The effect of temperature shift of reference arm on the demodulated temperature stability.

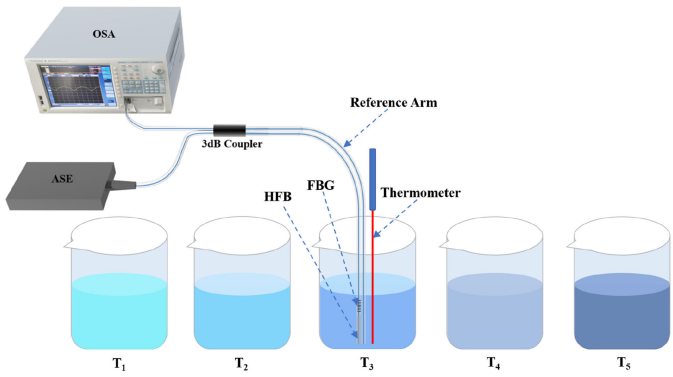

Fig. 6. Schematic view of the comparison test between the fiber sensor and thermometer.

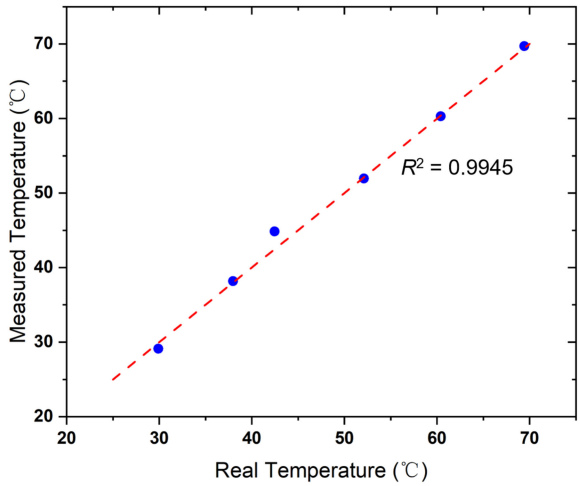

Fig. 7. The proposed fiber temperature sensor evaluation. The horizontal axis represents the temperature values measured by the standard platinum resistance thermometer. The vertical axis represents the values estimated by the fiber sensor. Dash line has unitary slope coefficient.

arm, which proves that our fiber sensor is immune to elements' instabilities.

B. Sensor Calibration and Evaluation

The introduction of the HBF enables a new demodulation scheme by measuring the fringe visibility for two beam interferometer and may provide a new interferometric sensing method with advantages including large measurement range, high accuracy and low cost. To verify the accuracy of this sensing method, temperature measurement is conducted as an example. We calibrate the sensor appropriately and carry out a comparison test based on the Michelson interferometer configuration sensor, as shown in Fig. 6.

First, we calibrate our sensor in a cup of water at different temperatures ranging from 30 to 80 °C. The real temperature is determined by a standard platinum resistance thermometer (Fluke.inc), which is submerged in the water side by side with the fiber sensor. Then we obtain a fitted curve, which enables the sensor to read temperature for a given visibility. Finally, several cups of water with different temperatures are measured by our sensor and the standard platinum resistance thermometer simultaneously. The comparison of the two readings is reported in Fig. 7. As shown in the figure, the demodulated temperature is well corelated with the real temperature except for one singularity, which is probably caused by the misreading. Since the fiber sensor and the thermometer cannot occupy the same position, minor variations in the measurement are unavoidable. Overall, the measurement accuracy is quite reasonable with the coefficients of determination (R^2) of 0.9945. The precision of the proposed temperature sensor would be better once the resolution of the thermometer used for calibration was improved. Moreover, we have tested the repeatability and stability of our sensor by measuring a temperature (30.2°C) at variable times, which are quite reasonable. In the future work, a more advanced thermometer and HBFs with higher birefringence will be considered to improve the sensor performance.

IV. Conclusion

In this paper, we proposed a demodulation scheme based on a Michelson interferometer configuration by measuring the

interference fringe visibility. The principle of demodulation scheme was validated theoretically and experimentally. Measurands were transferred into the visibility variation of the interference fringe during the experiments. Then, temperature sensing employing the Michelson interferometer configuration was presented as one of the potential applications. To the best of our knowledge, this is the first time to achieve reasonable temperature sensing by measuring interference fringe visibility. Its high performance as well as the immunities to instabilities, such as power fluctuation of light source, phase shift of the reference arm, noise of photo detector, and wavelength shift of OSA, indicate a promising candidate for low-cost and high precision interferometric sensing applications.

REFERENCES

[1] G. Gagliardi, M. Salza, S. Avino, P. Ferraro, and P. D. Natale, "Probing the ultimate limit of fiber-optic strain sensing," *Science*, vol. 330, no. 6007, pp. 1081–1084, 2010.

[2] I. Coddington, W. C. Swann, L. Nenadovic, and N. R. Newbury, "Rapid and precise absolute distance measurements at long range," *Nature Photon.*, vol. 3, no. 6, pp. 351–356, 2009.

[3] J. A. Blum, S. L. Nooner, and M. A. Zumberge, "Recording earth strain with optical fibers," *IEEE Sensors J.*, vol. 8, no. 7, pp. 1152–1160, Jul. 2008.

[4] R. M. Silva, M. S. Ferreira, J. L. Santos, and O. Frazao, "Nanostrain measurement using chirped Bragg grating Fabry-Perot interferometer," *Photonic Sensors*, vol. 2, no. 1, pp. 77–80, 2012.

[5] H. Gong, C. C. Chi, L. Chen, and X. Dong, "Strain sensor realized by using low-birefringence photonic-crystal-fiber-based sagnac loop," *IEEE Photon. Technol. Lett.*, vol. 22, no. 16, pp. 1238–1240, Aug. 2010.

[6] Y. Geng, X. Li, X. Tan, Y. Deng, and Y. Yu, "High-sensitivity Mach-Zehnder interferometric temperature fiber sensor based on a waist-enlarged fusion bitaper," *IEEE Sensors J.*, vol. 11, no. 11, pp. 2891–2894, Nov. 2011.

[7] R. Yang, Y. S. Yu, Y. Xue, C. Chen, Q. D. Chen, and H. B. Sun, "Single s-tapered fiber Mach-Zehnder interferometers," *Opt. Lett.*, vol. 36, no. 23, pp. 4482–4484, 2011.

[8] S. Wang *et al.*, "An infrasound sensor based on extrinsic fiber-optic Fabry-Perot interferometer structure," *IEEE Photon. Technol. Lett.*, vol. 28, no. 11, pp. 1264–1267, Jun. 2016.

[9] M. Yang and Y. Yang, "New measurement method for eigen frequency of a fiber optic gyroscope," *Opt. Eng.*, vol. 52, no. 2, 2013, Art. no. 0 24401.

[10] J. T. Kringlebotn, H. Nakstad, and M. Eriksrud, "Fibre optic ocean bottom seismic cable system: From innovation to commercial success," in *Proc. 20th Int. Conf. Opt. Fibre Sensors*, vol. 7503, 2009, Art. no. 75037U.

[11] G. A. Cranch, G. Flockhart, and C. K. Kirkendall, "Distributed feedback fiber laser strain sensors," *IEEE Sensors J.*, vol. 8, no. 7, pp. 1161–1172, Jul. 2008.

[12] S. Liu, Z. Yin, Z. Liang, L. Gao, and J. Cheng, "Multilongitudinal mode fiber laser for strain measurement," *Opt. Lett.*, vol. 35, no. 6, pp. 835–837, 2010.

[13] X. Ni, Z. Yong, and J. Yang, "Research of a novel fiber Bragg grating underwater acoustic sensor," *Sensors Actuators A. Phys.*, vol. 138, no. 1, pp. 76–80, 2007.

[14] Q. Liu, T. Tokunaga, and Z. He, "Ultra-high-resolution large-dynamic-range optical fiber static strain sensor using pound-drever-hall technique," *Opt. Lett.*, vol. 36, no. 20, pp. 4044–4046, 2011.

[15] J. Chen, Q. Liu, X. Fan, and Z. He, "Ultrahigh resolution optical fiber strain sensor using dual pound-drever-hall feedback loops," *Opt. Lett.*, vol. 41, no. 5, pp. 1066–1069, 2016.

[16] W. Huang, W. Zhang, T. Zhen, F. Zhang, and F. Li, "π-phase-shifted FBG for high-resolution static-strain measurement based on wavelet threshold denoising algorithm," *J. Lightw. Technol.*, vol. 32, no. 22, pp. 4294–4300, Nov. 2014.

[17] W. Huang, W. Zhang, T. Zhen, F. Zhang, and F. Li, "A cross-correlation method in wavelet domain for demodulation of FBG-FP static-strain sensors," *IEEE Photon. Technol. Lett.*, vol. 26, no. 16, pp. 1597–1600, Aug. 2014.

[18] J. Du and Z. He, "Sensitivity enhanced strain and temperature measurements based on FBG and frequency chirp magnification," *Opt. Exp.*, vol. 21, no. 22, pp. 27111–27118, 2013.

[19] C. Wang and J. Yao, "Ultrafast and ultrahigh-resolution interrogation of a fiber Bragg grating sensor based on interferometric temporal spectroscopy," *J. Lightw. Technol.*, vol. 29, no. 19, pp. 2927–2933, Oct. 2011.

[20] P. Malara *et al.*, "Enhanced spectral response of π-phase shifted fiber Bragg gratings in closed-loop configuration," *Opt. Lett.*, vol. 40, no. 9, pp. 2124–2126, 2015.

[21] W. Huang, W. Zhang, and F. Li, "Swept optical ssb-sc modulation technique for high-resolution large-dynamic-range static strain measurement using FBG-FP sensors," *Opt. Lett.*, vol. 40, no. 7, pp. 1406–1409, 2015.

[22] Q. Liu, T. Tokunaga, and Z. He, "Realization of nano static strain sensing with fiber Bragg gratings interrogated by narrow linewidth tunable lasers," *Opt. Exp.*, vol. 19, no. 21, pp. 20 214–20 223, 2011.

[23] L. Zhang, Y. Lu, Y. Dong, G. Jiao, W. Chen, and J. Lv, "An interferometric sensor based on visibility modulation," in *Proc. Fiber Opt. Sensors Appl. XIV*, vol. 10208, 2017, Art. no. 1020808.

[24] L. Zhang, Z. Zhu, M. Yin, and Y. Dong, "A large dynamic range interferometric fiber strain sensor," in *Proc. IEEE 18th Int. Conf. Opt. Commun. Netw.*, 2019, pp. 1–3.